Ni(II)·Arg-Gly-His−DNA Interactions: Investigation into the Basis for Minor-Groove Binding and Recognition

Ya-Yin Fang,[†] Bruce D. Ray,[‡] Craig A. Claussen,[†] Kenny B. Lipkowitz,[†,§] and Eric C. Long*,[†]

Contribution from the Departments of Chemistry and Physics, Purdue School of Science, Indiana University−Purdue University Indianapolis, Indianapolis, Indiana 46202

Received January 8, 2004; E-mail: long@chem.iupui.edu.

Abstract: A study of the minor-groove recognition of A/T-rich DNA sites by Ni(II)·L-Arg-Gly-His and Ni(II)·D-Arg-Gly-His was carried out with a fluorescence-based binding assay, one- and two-dimensional (1D and 2D) NMR methodologies, and molecular simulations. Fluorescence displacement titrations revealed that Ni(II)·L-Arg-Gly-His binds to A/T-rich sequences better than the D-Arg diastereomer, while NMR investigations revealed that both metallopeptides bind to the minor groove of an AATT core region as evidenced by an intermolecular nuclear Overhauser effect (NOE) between each metallopeptide His imidazole C4 proton and the C2 proton of adenine. Results from molecular dynamics simulations of these systems were consistent with the experimental data and indicated that the His imidazole N−H, the N-terminal peptide amine, and Arg side chains of each metallopeptide are major determinants of minor-groove recognition by functioning as H-bond donors to the O2 of thymine residues or N3 of adenine residues.

Introduction

Metallopeptides of the general form Cu(II)· or Ni(II)·Gly-Gly-His have contributed to our understanding of fundamental nucleic acid recognition and reactivity phenomena in the context of both proteins and low molecular weight agents.[1] These metallopeptides and their derivatives have been applied in the development of synthetic[2] or biosynthetic[3] affinity cleavage or activity-modulating[4] appendages to DNA-binding protein motifs and also occur in the native sequence of some DNA-associating proteins.[5] In addition, Gly-Gly-His-derived metallopeptides have served to model Ni-based toxicity and resultant DNA damage events,[6] have assisted in the development of low molecular weight drug,[7] oligonucleotide,[8] or PNA[9] conjugates, and as stand-alone metallotripeptides, have been agents to understand fundamental peptide and amino acid interactions with DNA or RNA.[10]

In the final area listed above, this laboratory has been exploiting the potential of Ni(II)·Gly-Gly-His-derived metallopeptides toward the understanding of DNA recognition by peptides and amino acids in a well-defined structural environment. Indeed, Cu(II)· or Ni(II)·Gly-Gly-His and derivatives, where Gly can be any α-amino acid, have historically served as models of the Ni(II) and Cu(II) transport domains of the serum albumins and exist as well-characterized, 1:1 transition metal complexes at physiological pH via chelation of the terminal peptide amine, two intervening deprotonated peptide amides, and the His imidazole with dissociation constants on the order of $10^{-16}-10^{-17}$.[11] Given their peptide-based composition, metallopeptides stand unique among metal-based nucleic acid binding agents in their ability to incorporate and position along the periphery of a well-defined metal complex framework the same chemical functional groups (e.g., guanidinium, amine, and amide moieties) used by proteins and peptide-based natural product antitumor agents for the molecular recognition of DNA and RNA.[12] In addition, the relative ease of individual or

  † Department of Chemistry.
  ‡ Department of Physics.
  § Present address: Department of Chemistry, North Dakota State University.

 (1) Long, E. C.; Claussen, C. A. In *DNA and RNA Binders: From Small Molecules to Drugs*; Demeunynk, M., Bailly, C., Wilson, W. D., Eds.; Wiley−VCH: New York, 2003; pp 88−125.
 (2) (a) Mack, D. P.; Iverson, B. L.; Dervan, P. B. *J. Am. Chem. Soc.* **1988**, *110*, 7572−7574. (b) Mack, D. P.; Dervan, P. B. *J. Am. Chem. Soc.* **1990**, *112*, 4604−4606. (c) Mack, D. P.; Dervan, P. B. *Biochemistry* **1992**, *31*, 9339−9405.
 (3) (a) Nagaoka, M.; Hagihara, M.; Kuwahara, J.; Sugiura, Y. *J. Am. Chem. Soc.* **1994**, *116*, 4085−4086. (b) Harford, C.; Narindrasorasak, S.; Sarkar, B. *Biochemistry* **1996**, *35*, 4271−4278.
 (4) Mahmoudi, T.; Sarkar, B. *Biopolymers* **1999**, *50*, 273−286.
 (5) (a) McKay, D. J.; Renaux, B. S.; Dixon, G. H. *Eur. J. Biochem.* **1986**, *156*, 5−8. (b) Bal, W.; Jezowska-Bojczuk, M.; Kasprzak, K. S. *Chem. Res. Toxicol.* **1997**, *10*, 906−914. (c) Bal, W.; Lukszo, J.; Kasprzak, K. S. *Chem. Res. Toxicol.* **1997**, *10*, 915−921. (d) Bal, W.; Wojcik, J.; Maciejczyk, M.; Grochowski, P.; Kasprzak, K. S. *Chem. Res. Toxicol.* **2000**, *13*, 823−830.
 (6) Muller, J. G.; Hickerson, R. P.; Perez, R. J.; Burrows, C. J. *J. Am. Chem. Soc.* **1997**, *119*, 1501−1506.

 (7) (a) Grokhovsky, S. L.; Nikolaev, V. A.; Zubarev, V. E.; Surovaya, A. N.; Zhuze, A. L.; Chernov, B. K.; Sidorova, N.; Zasedatelev, A. S. *Mol. Biol. (Moscow)* **1992**, *26*, 1274−1297. (b) Shullenberger, D. F.; Long, E. C. *Bioorg. Med. Chem. Lett.* **1993**, *3*, 333−336. (c) Morier-Teissier, E.; Boitte, N.; Helbecque, N.; Bernier, J. L.; Pommery, N.; Duvalet, J. L.; Fournier, C.; Hecquet, B.; Catteau, J. P.; Henichart, J. P. *J. Med. Chem.* **1993**, *36*, 2084−2090. (d) Steullet, V.; Dixon, D. W. *Bioorg. Med. Chem. Lett.* **1999**, *9*, 2935−2940.
 (8) (a) De Napoli, L.; Messere, A.; Montesarchio, D.; Piccialli, G.; Benedetti, E.; Bucci, E.; Rossi, F. *Bioorg. Med. Chem.* **1999**, *7*, 395−400. (b) Truffert, J.-C.; Asseline, U.; Brack, A.; Thuong, N. T. *Tetrahedron* **1996**, *52*, 3005−3016.
 (9) Footer, M.; Egholm, M.; Kron, S.; Coull, J. M.; Matsudaira, P. *Biochemistry* **1996**, *35*, 10673−10679.
(10) Long, E. C. *Acc. Chem. Res.* **1999**, *32*, 827−836.
(11) Harford, C.; Sarkar, B. *Acc. Chem. Res.* **1997**, *30*, 123−130.
(12) (a) Steitz, T. A. *Q. Rev. Biophys.* **1990**, *23*, 205−280. (b) Zimmer, C.; Wahnert, U. *Prog. Biophys. Mol. Biol.* **1986**, *47*, 31−112.

combinatorial peptide synthesis, the ability to readily alter the stereochemistry at select α-carbon centers, and their potential transformation into biosynthetic or peptidomimetic agents make Ni(II)·Gly-Gly-His derived metallopeptides attractive models to increase our knowledge of both protein− and drug−nucleic acid recognition events.

Ni(II)·Gly-Gly-His

Ni(II)·Arg-Gly-His

Ni(II)·Lys-Gly-His
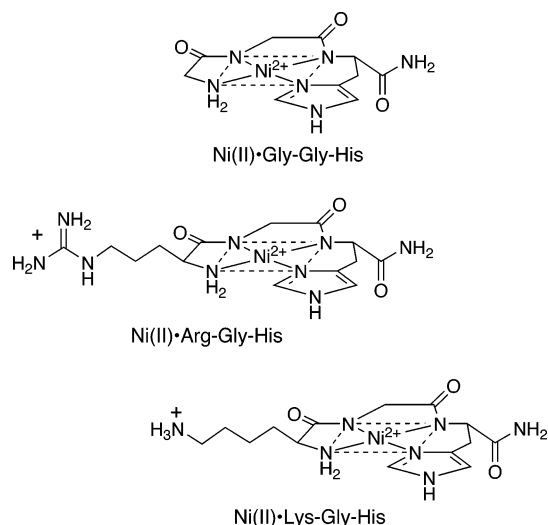
We have demonstrated previously that Ni(II)·Gly-Gly-His-derived metallopeptides containing carboxy-terminal amide moieties recognize and cleave DNA site-selectively as a function of their amino acid composition, chirality, and overall shape.[13] For example, inclusion of positively charged amino acids such as Arg or Lys focused the binding of these metallopeptides to A/T-rich DNA regions, while the inclusion of D-amino acids led to altered site selectivities. During the course of these investigations it became apparent that Ni(II)·Gly-Gly-His-derived metallopeptides likely bind DNA through a minor-groove recognition event. Evidence in support of minor-groove binding[13] includes a 3′-asymmetric DNA cleavage pattern, avoidance of homopolymeric $A_n \cdot T_n$ sites containing a narrowed minor groove, competition with distamycin, and direct DNA strand scission through a C4′-H abstraction mechanism.[14] In addition, recent DNA fiber electron paramagnetic resonance (EPR) structural investigations of Cu(II)·Xaa-Gly-His (where Xaa is Gly, Arg, or Lys) have demonstrated that the $g_{\parallel}$ axes and mean equatorial planes of these metallopeptides are tilted approximately 50° and 40°, respectively, relative to the DNA fiber axis, suggesting a stereospecific orientation in the minor groove.[15]

The studies described above, along with a combinatorial investigation[16] that revealed amino acid substitutions for the Gly residues of Ni(II)·Gly-Gly-His, which appear prominently in minor-groove binding protein motifs (e.g., A·T-hooks[17]), sug-

gested a plausible model of DNA minor-groove binding in which the amino-terminal nitrogen and the His imidazole ring "edge" of the approximately square planar structure inserts into the minor groove; this binding mode would permit the formation of H-bonds between a unique "metal-activated" His imidazole pyrrole N−H,[18] the terminal amine N−H protons, and prominent H-bond acceptors on the floor of the minor groove in A/T-rich regions (i.e., the O2 of thymine and the N3 of adenine). In further support of this model, we have found that Ni(II)·Gly-Gly-His-derived metallopeptides with N3 methylated His residues do not interact with DNA.[19]

Ni(II)·Gly-Gly-His metallopeptides thus serve as "minimalist" protein models to further our understanding of fundamental DNA recognition events and the design of DNA binding agents through the use of Nature's molecular recognition "toolbox", in particular the role of His as a potential hydrogen-bond donor and the behavior and influence of positively charged residues delivered to the minor-groove. Of relevance, imidazole moieties and pendant, positively charged functional groups have contributed to the development of pyrrole−imidazole polyamides[20] and microgonotropens,[21] underscoring the importance of their investigation in the search for improved agents[22] in the context of alternative structures. Accordingly, we have sought to characterize the DNA minor-groove binding of Ni(II)·L/D-Arg-Gly-His metallopeptides through fluorescence titration, one- and two-dimensional (1D and 2D) NMR methodologies, and molecular simulations with the aim of understanding more fully the role of amino acid side chains and their α-carbon stereochemistry in the minor-groove recognition process.

Results and Discussion

Fluorescence Titrations. Given the underlying A/T-selective cleavage[23] exhibited by positively charged Ni(II) metallopeptides, the binding of Ni(II)·L-Arg-Gly-His and Ni(II)·D-Arg-Gly-His to a series of dodecanucleotide substrates containing A/T cores was studied. The oligonucleotide sequences examined were based on the well-characterized Dickerson dodecanucleotide[24] 5′-CGCGAATTCGCG and contained the original AATT sequence or three symmetrical variations of it (ATAT, TATA, or TTAA) within the context of four flanking G·C base pairs.[25] This initial survey was conducted to establish (1) if any distinct sequence or structural prerequisites for metallopeptide A/T-selectivity exist, including altered patterns of minor-groove

(13) Liang, Q.; Eason, P. D.; Long, E. C. *J. Am. Chem. Soc.* **1995**, *117*, 9625−9631.
(14) Liang, Q.; Ananias, D. C.; Long, E. C. *J. Am. Chem. Soc.* **1998**, *120*, 248−257.
(15) Nagane, R.; Koshigoe, T.; Chikira, M.; Long, E. C. *J. Inorg. Biochem.* **2001**, *83*, 17−23.
(16) Huang, X.; Pieczko, M. E.; Long, E. C. *Biochemistry* **1999**, *38*, 2160−2166.
(17) (a) Reeves, R.; Nissen, M. S. *J. Biol. Chem.* **1990**, *265*, 8573−8582. (b) Huth, J. R.; Bewley, C. A.; Nissen, M. S.; Evans, J. N. S.; Reeves, R.; Gronenborn, A. M.; Clore, G. M. *Nat. Struct. Biol.* **1997**, *4*, 657−665. (c) Banks, G. C.; Mohr, B.; Reeves, R. *J. Biol. Chem.* **1999**, *274*, 16536−16544.

(18) Sundberg, R. J.; Martin, R. B. *Chem. Rev.* **1974**, *74*, 471−517.
(19) Eason, P. D. Ph.D. Dissertation, Purdue University, West Lafayette, IN, 1997.
(20) Dervan, P. B.; Edelson, B. S. *Curr. Opin. Struct. Biol.* **2003**, *13*, 284−299.
(21) Satz, A. L.; Bruice, T. C. *Acc. Chem. Res.* **2002**, *35*, 86−95.
(22) Renneberg, D.; Dervan, P. B. *J. Am. Chem. Soc.* **2003**, *125*, 5707−5716.
(23) A/T-selective DNA *cleavage* by these metallopeptides has been established. In addition, metallopeptide titrations performed with a series of bulk DNA substrates including calf thymus DNA in comparison to poly(ApT), poly-(GpC), and poly(IpC) revealed a 2−3-fold preference in binding affinities for poly(ApT) by each metallopeptide; titrations with poly(GpC) vs poly-(IpC) were essentially indistinguishable, suggesting that the exocyclic amino group of guanine alone does not limit metallopeptide selectivity for G/C-rich regions through simple steric exclusion.
(24) (a) Wing, R. M.; Drew, H. R.; Takano, T.; Broka, C.; Tanaka, S.; Itakura, K.; Dickerson, R. E. *Nature* **1980**, *287*, 755−758. (b) Neidle, S. *Nat. Prod. Rep.* **2001**, *18*, 291−309.
(25) While some have argued that tetranucleotide sequences alone do not define a local DNA structure, as noted,[26] isolated di-, tri-, and tetranucleotide A/T sequences are targeted in cleavage-based assays of metallopeptide sequence selectivity.
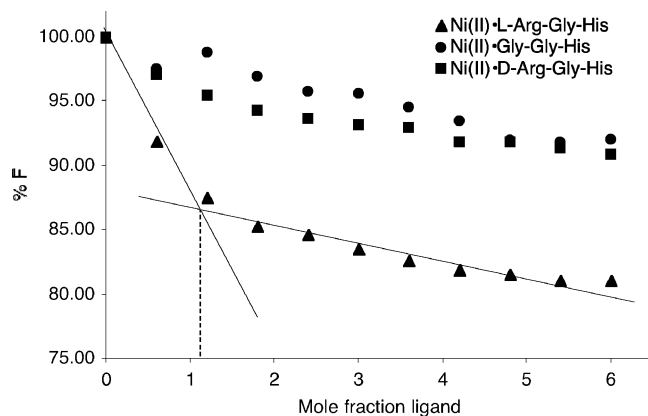
Figure 1. Fluorescence intercalator displacement titrations of Ni(II)·L/D-Arg-Gly-His binding to d(CGCGAATTCGCG)$_2$. Intersecting lines in the titration plot emphasize the approximate 1:1 binding stoichiometry exhibited by Ni(II)·L-Arg-Gly-His.

Table 1. Metallopeptide−Oligonucleotide Binding Affinities ($K_a \times 10^6$ M^{-1})

	AATT	TTAA	ATAT	TATA
Ni(II)·L-Arg-Gly-His	3.8	0.7	1.8	3.0
Ni(II)·D-Arg-Gly-His	1.4			

H-bond acceptors and the presence of ApT vs TpA steps; (2) a comparison to other nonmetallopeptide A/T-selective binders[26] such as netropsin, distamycin, and Hoechst dye; and (3) preferred oligonucleotide−metallopeptide binding pair(s) for further investigations.

For the oligonucleotide substrates listed above, fluorescence displacement[27] titrations employing ethidium bromide were carried out as a function of added metallopeptide followed by Scatchard analyses[28−30] of the data obtained; taking into consideration the limitations associated with such an assay,[27−30] we regard these measurements mainly as a means to assess the relative binding affinities of each ligand studied. Fluorescence displacement plot curvature and reasonable fit Scatchard analyses indicative of 1:1 binding were observed to occur within only a subset of the four sequences examined (Figure 1 and Supporting Information); for other binding pairs, the resulting titration curves did not exhibit 1:1 binding sufficient to yield well-defined Scatchard plots, indicating only weak, nonselective binding.

Among the sites examined, the AATT core sequence (Figure 1) presented the best 1:1 binding site for Ni(II)·L-Arg-Gly-His based on direct fluorescence displacement plots and Scatchard transformations; the 15−17% decrease in fluorescence observed suggested the displacement of ∼1−2 ethidium bromides from the dodecanucleotide substrate, as expected. In comparison, Ni(II)·D-Arg-Gly-His exhibited reduced binding (Table 1 and Supporting Information) and, for comparison, Ni(II)·Gly-Gly-His did not associate measurably with the AATT oligonucleotide. Further, with the TTAA, ATAT, and TATA sequences, Ni(II)·L-Arg-Gly-His was observed to bind to each, albeit to

lesser extents in comparison to AATT, producing reasonable fluorescence plot curvature and Scatchard binding isotherms (Table 1 and Supporting Information). Thus, while Ni(II)·L-Arg-Gly-His bound to the sites examined in the approximate preferred order AATT > TATA > ATAT > TTAA, Ni(II)·D-Arg-Gly-His was observed to bind appreciably to AATT only. These data (Table 1) also indicate that Ni(II)·L-Arg-Gly-His binds to the sequences examined to an extent that is 4−20-fold less than the affinity displayed by netropsin for similar oligonucleotides;[29] the extent of fluorescence displacement plot curvature produced by Ni(II)·L-Arg-Gly-His was also reminiscent of that displayed by the minor-groove binding agent berenil.[30]

The above analyses indicate that the metallopeptides examined can discriminate among available A/T-rich tetranucleotide binding sites, a finding that is clear from previous cleavage-based studies[13,14] yet not established through a binding-only assay until now, and that both the presence and α-carbon stereochemistry of Arg residues influenced binding to these substrates. Additionally, in a fashion that parallels the binding preferences of most nonmetallopeptide A/T-selective DNA-binding small molecules,[26] (1) AATT sites with a narrowed minor groove containing a spine of hydration appear to be preferred for the L-Arg- and D-Arg-containing metallopeptides and (2) different sequential arrangements of A·T base pairs lead to varied affinities; with Ni(II)·L-Arg-Gly-His, ATAT is preferred over TTAA like other minor-groove binders, a preference generally attributed to the narrower minor-groove width of ATAT.[24a,26] Differing, however, from the trends exhibited by some minor-groove binders, Ni(II)·L-Arg-Gly-His binds to TATA sites with a preference over ATAT and TTAA, suggesting that this metallopeptide may be sensitive to sites containing central TpA steps known to disrupt and reduce the binding affinity of A/T-targeted agents[31] such as netropsin and bisbenzimidazoles. Thus, these findings establish that the Ni(II)·metallopeptides recognize and discriminate different A/T-rich tracts like other low molecular weight agents. In doing so, these metallopeptides exhibit a level of subtle variation that distinguishes them from other agents but remains in common with the variability observed to occur between the other diverse structures that target these DNA regions.[26] Most importantly, these data establish that the AATT sequence presents a binding site for Ni(II)·L-Arg-Gly-His and Ni(II)·D-Arg-Gly-His that leads to an association with an apparent 1:1 stoichiometry.

NMR Investigations. Given the ability of Ni(II)·L-Arg-Gly-His and Ni(II)·D-Arg-Gly-His to bind to the AATT site and also the well-characterized nature of this oligonucleotide,[24,32,33] qualitative NMR studies were pursued to understand the binding location and orientation of these metallopeptides upon oligonucleotide association. Shown in Figure 2 are 1D spectra acquired during the course of a titration of the AATT oligonucleotide with a 1:1 complex of Ni(II)·L-Arg-Gly-His along with a spectrum of Ni(II)·L-Arg-Gly-His alone; the 1D spectra obtained in the corresponding titration with Ni(II)·D-Arg-Gly-

(26) Abu-Daya, A.; Brown, P. M.; Fox, K. R. *Nucleic Acids Res.* **1995**, *23*, 3385−3392.
(27) Jenkins, T. C. In *Drug−DNA Interaction Protocols*; Fox, K. R., Ed.; Methods in Molecular Biology; Humana Press: Totowa, NJ, 1997; Vol. 90, pp 195−218.
(28) Scatchard, G. *Ann. N.Y. Acad. Sci.* **1949**, *51*, 660−672.
(29) Boger, D. L.; Tse, W. C. *Bioorg. Med. Chem. Lett.* **2001**, *9*, 2511−2518.
(30) Boger, D. L.; Fink, B. E.; Brunette, S. R.; Tse, W. C.; Hedrick, M. P. *J. Am. Chem. Soc.* **2001**, *123*, 5878−5891.

(31) (a) Ward, B.; Rehfuss, R.; Goodisman, J.; Dabrowiak, J. C. *Biochemistry* **1988**, *27*, 1198−1205. (b) Chen, F. M.; Sha, F. *Biochemistry* **1998**, *37*, 11143−11151. (c) Satz, A. L.; White, C. M.; Beerman, T. A.; Bruice, T. C. *Biochemistry* **2001**, *40*, 6465−6474.
(32) Rajagopal, P.; Gilbert, D. E.; van der Marel, G. A.; van Boom, J. H.; Feigon, J. *J. Magn. Reson.* **1988**, *78*, 526−537.
(33) Hare, D. R.; Wemmer, D. E.; Chou, S.-H.; Drobny, G.; Reid, B. R. *J. Mol. Biol.* **1983**, *171*, 319−336.
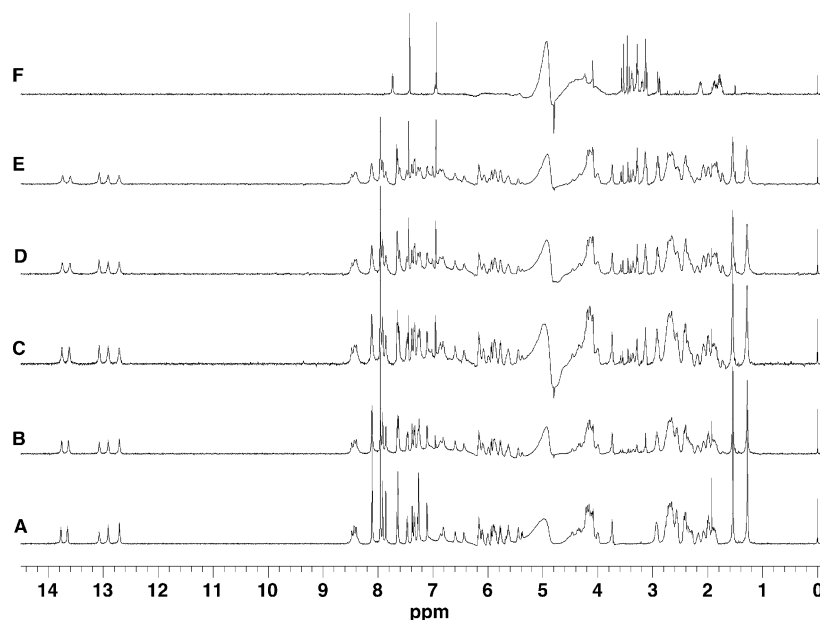
Figure 2. Titration of duplex 5′-$C_1G_2C_3G_4A_5A_6T_7T_8C_9G_{10}C_{11}G_{12}$ at 25 °C with a 1:1 complex of Ni(II)·L-Arg-Gly-His. Sample conditions are as stated in the Experimental Section. NMR conditions for all spectra: sweep width, 10 750 Hz; pulse width, 8.65 μs; recycle delay, 3 s; number of complex data points, 8192. (A) DNA alone, 64 transients; (B) DNA:Ni(II)·L-Arg-Gly-His 1:0.5, 64 transients; (C) DNA:Ni(II)·L-Arg-Gly-His 1:1, 64 transients; (D) DNA:Ni(II)·L-Arg-Gly-His 1:1.5, 64 transients; (E) DNA:Ni(II)·L-Arg-Gly-His 1:2, 64 transients; (F) Ni(II)·L-Arg-Gly-His alone, 128 transients.

His were essentially identical to those shown here. During the course of these titrations, only minor chemical shift changes of less than 0.05 ppm were observed for either the metallopeptide or the DNA. In these spectra, several changes upon titration were immediately evident. First, while the G·C base pair imino proton resonances were differentially affected by increases in the metallopeptide:DNA ratio, the A_6·T_7 and A_5·T_8 base-pair imino proton resonances, located at 13.65 and 13.77 ppm, respectively, were broadened equally. With the G·C imino proton resonances, the G_4·C_9 resonance at 12.71 ppm was the most broadened by metallopeptide binding, while that for the G_2·C_{11} base pair at 13.07 ppm appeared to be least affected, with the G_{10}·C_3 base-pair resonance at 12.91 ppm affected to an intermediate extent. The C_1·G_{12} base-pair imino resonances at the termini of the oligonucleotide, extensively exchange-broadened due to their location, were not observed, as was reported previously.[32] In contrast to the imino protons, the cytosyl C4 amino protons involved in hydrogen bonding, observed between 8.35 and 8.45 ppm, appeared to be only slightly affected by the addition of the metallopeptide.

In comparison to the exchangeable resonances discussed above, with the nonexchangeable aromatic nucleobase protons, the C8 protons of A_5 and A_6, seen at 8.09 ppm, broadened with increased Ni(II)·Arg-Gly-His, while the equivalent C8H guanyl resonances from G_2 and G_{12}, observed between 7.9 and 7.92 ppm, were much less affected. Finally, both thymine C5-methyl resonances were broadened with increased Ni(II)·peptide, with the T_7 methyl at 1.28 ppm appearing to be more affected than the T_8 resonance at 1.54 ppm. The broadening observed with these nonexchangeable protons suggests that the T_7 methyl and the adenine C8Hs are in closer proximity to the Ni(II) center than the T_8 methyl, the G_2 and G_{12} guanyl C8Hs, or the cytosyl aminos. Given the minimal effect observed with the nonexchangeable G/C protons, the G·C imino resonances mentioned earlier likely experienced exchange broadening due to structural changes in the oligonucleotide upon metallopeptide binding to

the AATT core. The results from the titrations described above, taken together, indicate that the Ni(II) center of the metallopeptide lies in close proximity to the dyad axis contained within the AATT core of the oligonucleotide substrate. Meanwhile, the G/C-rich flanks of the oligonucleotide likely are affected by structural perturbations leading to exchange broadening as a function of distance from the metallopeptide-bound AATT core.

In addition to 1D experiments, 2D experiments were also conducted. Initially, a reference spectrum of duplex 5′-CGC-GAATTCGCG without added metallopeptide was generated at 25 °C (Supporting Information) and was found to be comparable to those published by Rajagopal et al.[32] Upon metallopeptide titration, the strong C_3 intraresidue H2″ to H6 cross-peak at 7.24 by 2.22 ppm was lost at a ratio of DNA:metallopeptide of 1:1. However, the interresidue G_2 H2″ to C_3 H6 cross-peak at 7.24 by 2.68 ppm remained, indicating that loss of the C_3 intraresidue cross-peak was not from simple relaxation of the C_3 H6 and suggesting that a change in the C_3 glycosidic angle occurs upon metallopeptide binding. In support of a proposed metallopeptide-induced oligonucleotide structural change in this region, the G_4·C_9 to A_5·T_8 imino–imino interresidue cross-peak also was weakened significantly. The above results are therefore consistent with the 1D spectral changes that suggested a structural alteration within the G/C flanks leading to imino proton exchange broadening.

In a further detailed analysis of the 2D spectra generated, the region indicated as D by Rajagopal et al.[32] for the duplex oligonucleotide alone and in the presence of Ni(II)·L-Arg-Gly-His at 25 °C were compared as shown in Figure 3. In the presence of the peptide-bound Ni(II), water relaxation times were decreased suggesting some population of paramagnetic Ni, which places greater demands on the water suppression and on the solvent subtraction method. Titration of the DNA with metallopeptide permitted separation of DNA intramolecular cross-peaks from those that arose either from DNA-bound
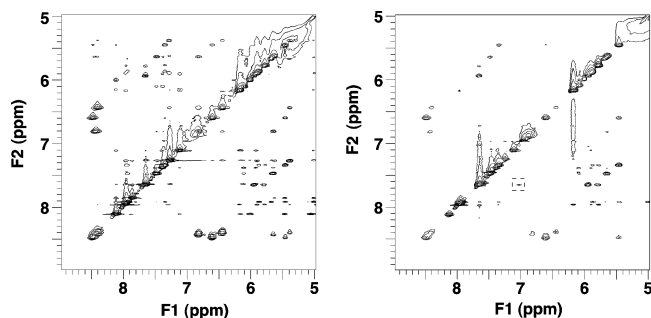
Figure 3. Comparison of NOESY spectra of DNA alone (left) to a 1:1 DNA:Ni(II)·L-Arg-Gly-His complex (right) at 25 °C. Sample conditions are given in the Experimental Section. NMR conditions: sweep width in both dimension, 10 750 Hz; pulse width, 8.65 μs; recycle delay, 1 s; number of complex data points in $f2$, 1024; number of increments in $f1$, 256; number of transients, 64 (left spectrum) and 32 (right spectrum). Processing parameters: apodization in $f2$, 80° shifted sin^2; apodization in $f1$, Gaussian at 0.0238 Hz^{-1}; linear prediction in $f2$, double acquired points; linear prediction in $f1$, triple acquired increments.
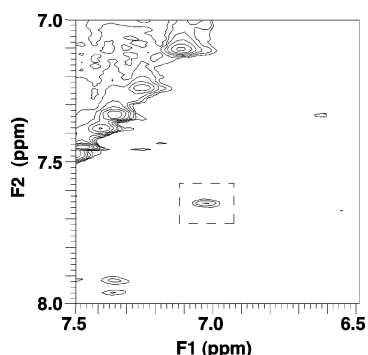
Figure 4. Enlargement of the region around the intermolecular cross-peak seen in the 1:1 DNA:Ni(II)·peptide complex NOESY. Sample conditions were as given in the text; NMR and processing conditions were as given in the caption to Figure 3.

metallopeptide intramolecular or from DNA−metallopeptide intermolecular interactions. Neither the peptide alone nor the Ni(II)·peptide complex alone produced NOE cross-peaks; the only ROE cross-peaks seen for the peptide and for the Ni(II)· peptide complex were those for intraresidue side-chain nearest neighbors. Therefore, new cross-peaks that appeared upon titration of the duplex oligonucleotide with the Ni(II)·Arg-Gly-His complexes were a consequence of binding to the DNA substrate.

Significantly, upon metallopeptide−oligonucleotide association, a moderate-intensity cross-peak appeared that connects 7.64 and 7.01 ppm, the positions of the adenyl H2 of A_6 and the His imidazole ring C4 proton of Ni(II)·Arg-Gly-His (see Figure 3 and an expansion of this region in Figure 4); this cross-peak increased in intensity as a function of added metallopeptide. Thus the His imidazole ring C4 proton is approximately 5−6 Å from the A_6 adenyl C2H, located on the floor of the minor groove, verifying that the His imidazole ring is inserted into the minor groove of the AATT core and in close proximity to the groove floor. In addition, upon titration with each metallopeptide, a number of DNA intramolecular cross-peaks in the H8, H6 to H1' region and the cross-peaks for C4H-1 and -2 intraresidue interactions, both between themselves and with H5 for C_3 and C_9, were weakened while those involving C_{11} were not. Because Ni(II) is bound to the His ring shown to be in close proximity to A_6, the weakening of these intraresidue interactions on the major-groove side of the G·C base pairs from

the distant minor-groove-bound His ring and Ni(II) most likely, again, represents a slight deformation of the DNA backbone and base-pair planes. The above is consistent with the disruption of the other cross-peaks noted above (e.g., the C_3 intraresidue cross-peak) and the analysis of the 1D spectra.

Overall, these NMR studies confirm that the Ni(II)-bound His imidazole moiety is inserted into the minor groove of the AATT core of this oligonucleotide target close to the A_6 C2H. In this orientation, binding of the Ni(II) metallopeptide broadens the resonances in close proximity. In addition, these data suggest that metallopeptide binding to the AATT core also induces a structural alteration within the G·C base pairs flanking the AATT core, leading to increased exchange broadening that diminishes as a function of distance from the AATT core.

Modeling and Simulations. A computational examination of Ni(II)·L-Arg-Gly-His and Ni(II)·D-Arg-Gly-His binding to the minor groove of d(CGCGAATTCGCG)$_2$ was carried out through molecular modeling and simulation protocols similar to those employed by Wellenzohn and co-workers.[34−36] As a starting point for these investigations, a crystal structure[37] of netropsin-bound d(CGCGAATTCGCG)$_2$ was used to create a minor-groove binding site by replacing netropsin with one or the other above metallopeptides. Given the similarities between netropsin and Ni(II)·Arg-Gly-His metallopeptides with regard to their minor groove site selectivities and fundamental chemical and steric features, the crystal structure of DNA bound by netropsin provides a convenient and realistic initial structure to assist in these investigations.

The metallopeptide starting structures used in these studies (Supporting Information) were based on the crystal structure[38] of Ni(II)·Gly-Gly-His, and force-field parameters were developed for that tripeptide complexed with Ni(II) (Supporting Information). Each metallopeptide, containing either an L-Arg or D-Arg side chain in the first amino acid position, was then docked manually at the dyad axis of the oligonucleotide substrate with the N-terminal amine and imidazole edge of each complex inserted into the minor groove. The docked starting structures were generated *independently* of the 1D and 2D NMR data described earlier but took into consideration all other information available to date, including data from cleavage chemistry and EPR fiber studies. Constraints based on observed NOEs were *not* used in generation of these starting structures, nor were any constraints employed during the course of the modeling and simulations. Worthy of note, the distance between the His imidazole C4 proton exhibiting an NOE cross-peak to the A_6 C2H was approximately 4−5 Å for both metallopeptide isomers in these starting structures, suggesting a close correspondence to the NMR data discussed earlier. Electroneutrality of each docked structure was achieved through the addition of 21 Na$^+$ counterions by standard procedures to balance the 11 phosphate anions provided by each single strand of DNA and the positively charged metallopeptide. Subsequently, solvation of each DNA

(34) Wellenzohn, B.; Winger, R. H.; Hallbrucker, A.; Mayer, E.; Liedl, K. R. *J. Am. Chem. Soc.* **2000**, *122*, 3927−3931.
(35) Wellenzohn, B.; Flader, W.; Winger, R. H.; Hallbrucker, A.; Mayer, E.; Liedl, K. R. *Biophys. J.* **2001**, *81*, 1588−1599.
(36) Flader, W.; Wellenzohn, B.; Winger, R. H.; Hallbrucker, A.; Mayer, E.; Liedl, K. R. *J. Phys. Chem. B* **2001**, *105*, 10379−10387.
(37) Sriram, M.; van der Marel, G. A.; Roelen, H. L.; van Boom, J. H.; Wang, A. H. J. *Biochemistry* **1992**, *31*, 11823−11834.
(38) Bal, W.; Djuran, M. I.; Margerum, D. W.; Gray, E. T.; Mazid, M. A.; Tom, R. T.; Nieboer, E.; Sadler, P. J. *J. Chem. Soc., Chem. Commun.* **1994**, 1889−1890.

Table 2. Relative Binding Energies of Ni(II)·Arg-Gly-His[a]

	Ni(II)·L-Arg-Gly-His				Ni(II)·D-Arg-Gly-His			
	$E_{complex}$[b]	E_{DNA}[b]	E_{ligand}[b]	ΔE[c]	$E_{complex}$[b]	E_{DNA}[b]	E_{ligand}[b]	ΔE[c]
1,4-EEL	−3391.82	−3184.79	−207.00		−3396.48	−3195.06	−201.41	
1,4VDW	210.15	204.21	5.94		208.09	202.09	5.99	
angle	592.42	409.76	182.66		591.66	409.23	182.43	
bond	209.707	197.60	12.09		208.33	196.44	11.88	
dihedral	500.97	446.58	54.39		496.00	439.59	56.41	
EEL	3081.44	3592.51	78.87	−589.93	3128.12	3624.96	78.34	−575.18
VDW	−450.75	−405.01	−4.94	−40.79	−442.64	−404.48	−4.94	−33.21
total	752.141	1260.88	122.02	−630.76	793.08	1272.77	128.71	−608.40

[a] Energies are reported in kilocalories per mole. [b] $E_{complex}$, E_{DNA}, and E_{ligand} denote the molecular mechanical (MM) energies for the complex, DNA, and ligand, respectively. [c] Relative binding energies, calculated by $\Delta E = E_{complex} - E_{DNA} - E_{ligand}$.
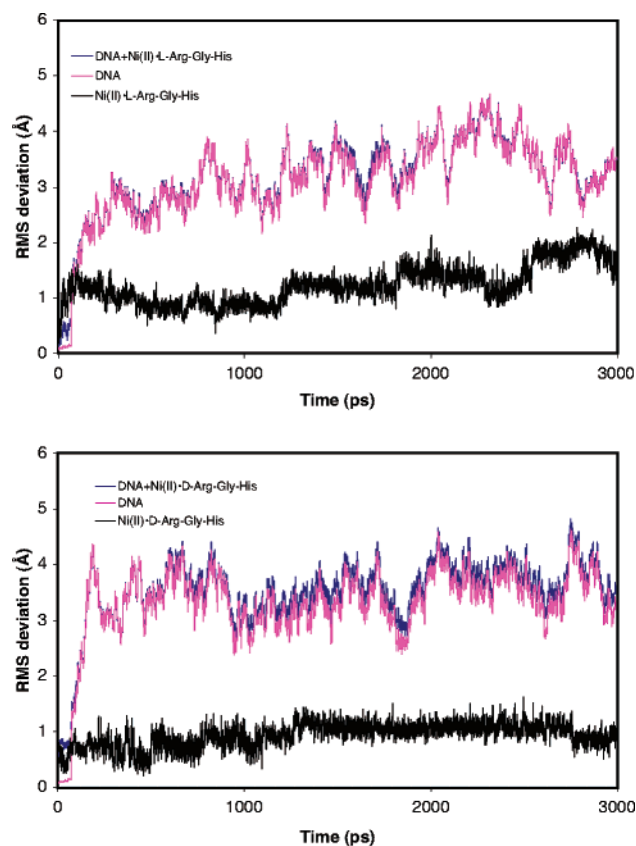
Figure 5. RMS deviations with respect to the starting structures in simulations of Ni(II)·L-Arg-Gly-His (top) and Ni(II)·D-Arg-Gly-His (bottom) bound to d(CGCGAATTCGCG)$_2$.

complex was achieved by use of a TIP3P water box that provided a 10 Å solvent shell in all directions, resulting in systems with dimensions 57.63 × 69.84 × 50.12 Å^3 and 48.41 × 67.01 × 63.09 Å^3 containing 4871 and 4875 waters, respectively; corresponding Γ values (water/nucleotide) were 202.95 and 203.12.

Upon energy minimization and molecular dynamics (MD) equilibration of each starting structure, the energy of the system stabilized for the remainder of the simulation. As shown in Figure 5, the root-mean-squared (RMS) deviation of the DNA + metallopeptide complex, the DNA alone, and the metallopeptide alone with respect to their starting structures attained equilibrium after 250 ps, hence 500 ps after thermal warm-up was selected as a starting point for data collection for each simulation. Attesting to the validity of these simulations, (1) the calculated binding energies for Ni(II)·L-Arg-Gly-His and Ni(II)·D-Arg-Gly-His to the AATT oligonucleotide (Table 2)

paralleled the experimental observations derived from the fluorescence assay described earlier and (2) the distances measured from the His imidazole C4 protons of the L-Arg and D-Arg metallopeptide isomers to the A$_6$ C2 protons of the duplex substrate after 3 ns of simulation time were, respectively, 3−5 and 5−6 Å, corresponding closely to the distances required for the observation of their intermolecular NOEs.

RMS deviations were used to assess the relative motion of the DNA-bound ligands in a cursory examination of each simulation. In the calculation of DNA + Ni(II)·L-Arg-Gly-His, the RMS deviations of this complex and those of the DNA backbone alone coincided, suggesting that Ni(II)·L-Arg-Gly-His fits snugly in the minor groove with very little independent motion. With Ni(II)·D-Arg-Gly-His, in contrast, the RMS value of the DNA + metallopeptide complex deviated consistently (ca. 0.2 Å) from that of the DNA alone, indicating that the complex formed between the D-Arg metallopeptide isomer and the DNA minor groove was less stable and that the metallopeptide shifted position relative to the DNA during the course of the simulation. The differences between these two metallopeptide isomers are emphasized also by the RMS values calculated for each metallopeptide when bound to the minor groove. As illustrated in Figure 5, the RMS deviations of Ni(II)·L-Arg-Gly-His were larger (ca. 1.46 Å) than those of Ni(II)·D-Arg-Gly-His (ca. 1.0 Å), indicating that the L-Arg isomer maintained a better overall complementary fit with the DNA during the course of the simulation, i.e., as the DNA moved, the metallopeptide was capable of complementary motions due to the maintenance of a stronger interaction with the groove structure. With the D-Arg isomer, the smaller RMS deviations indicated that this DNA-bound metallopeptide remained more independent of the DNA groove, a result arising from a weakened intermolecular interaction, which is consistent with the titration data described earlier.

Further analysis of the trajectory supports the general observations described above and reveals details of each metallopeptide−minor-groove binding interaction. With Ni(II)·L-Arg-Gly-His, a stable complex was formed with the DNA that did not reposition with respect to the DNA minor groove upon thermal equilibration. In the minor-groove-bound structure of Ni(II)·L-Arg-Gly-His, the coordination plane of the metallopeptide (i.e., all portions of the metallopeptide except for the side chain of the Arg residue) remained almost parallel to, and equidistant between, the walls of the minor groove within the AATT core region (Figure 6). Within this complex, the pyrrole N−H of the His imidazole moiety is in close proximity to three prominent H-bond acceptors located on the floor of
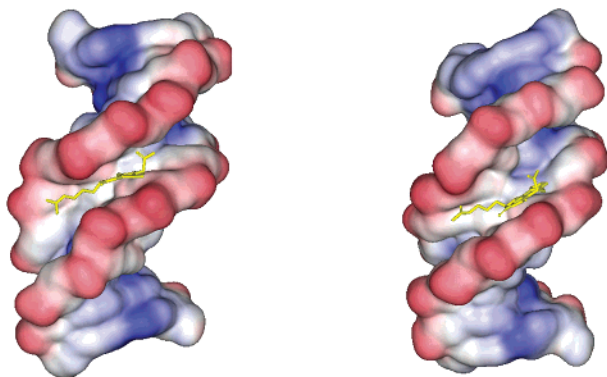
Figure 6. Space-filling DNA models of average structures resulting from simulations of Ni(II)·L-Arg-Gly-His (left) and Ni(II)·D-Arg-Gly-His (right) with d(CGCGAATTCGCG)$_2$ emphasizing the relative orientation of each metallopeptide with the DNA minor groove and the resulting groove widths.

the minor groove (see Figure 7): the O2 of T$_7$, the O2 of T$_8$, and the N3 of A$_6$′ (primed nucleotides indicate those contained within the complementary duplex strand). During the course of the simulation, the imidazole N−H hydrogen formed bonds to all three of these acceptor atoms with a distinct preference for the O2 of T$_8$ (∼50% of the total simulation time). The distance found between the His imidazole C4 proton and the minor-groove A$_6$′-C2 proton ranges from 3 to 5 Å in this orientation, entirely consistent with the intermolecular NOE observed in our parallel NMR investigation. Along with the His residue, the two N-terminal amine protons of the metallopeptide core are located approximately in the middle of the AATT sequence allowing hydrogen bonds to form to the O2 of either T$_7$ or T$_7$′ on antiparallel strands of the duplex (see Figure 7). In addition, while maintaining the primary interactions described above, the C-terminal amide N−H of the metallopeptide generates weaker, transient points of contact with the DNA backbone via the phosphate of C$_9$ or with the phosphate group of the T$_8$′ residue through a small tilting of the complex in the minor groove.

Overall, the hydrogen bonds described above serve to lock the equatorial plane of Ni(II)·L-Arg-Gly-His into the AATT core region, forming a tight "sandwich" with the walls of the minor groove, narrowing the distance between the walls to 9.7 Å in comparison to the unbound DNA structure (10.4 Å)[35] (Figure 6); this observation also compares quite favorably to the narrowing of the minor groove caused by netropsin binding in the same region (9.8 Å). The results of these simulations also revealed that the Ni(II) center of the metallopeptide coordination plane is located approximately 4 Å from the C4′-H of T$_8$ and T$_8$′ located on the complementary strands of the duplex (Figure 7); abstraction of these protons would lead to DNA cleavage with the characteristic 3′-asymmetric patterns observed experimentally.[1,10] In addition, the distances from the Ni(II) center to the T$_7$ and T$_8$ C5-methyl groups were 5.54 and 6.71 Å, respectively, again consistent with the NMR data noted previously.

In comparison to the coordination plane of the metallopeptide, the L-Arg side chain of Ni(II)·L-Arg-Gly-His, containing a positively charged guanidinium functionality, was found to extend beyond the AATT core to the junction between the G$_4$·C$_9$′ and A$_5$·T$_8$′ base pairs. This moiety of the metallopeptide remained relatively mobile yet still within the walls of the minor groove, in an orientation similar to the guanidinium moiety of netropsin in its crystal structure[37] with the same AATT oligonucleotide (80% of the simulation time). The minor groove was observed to widen (A$_6$ to G$_{10}$′ distance) in proximity to the guanidinium tail of Ni(II)·L-Arg-Gly-His, (Figure 6) due to B$_I$ phosphate[36] formation at A$_6$ and G$_{10}$′, a result similar to that observed[34,35] with netropsin; these simulations also indicated that the C$_3$·G$_{10}$ and G$_4$·C$_9$ base pairs were slightly altered in this location, consistent with the structural changes in the G/C base pairs flanking the AATT core suggested by the NMR data. While the Arg guanidinium tail of Ni(II)·L-Arg-Gly-His appears more flexible than the coordination plane of the metallopeptide, it was found to form transient hydrogen bonds via the δN−H to the N3 positions of the A$_5$ and A$_6$ residues (Figure 7) and to interact weakly, via the terminal positively charged N−H protons, with the phosphate groups of A$_5$, A$_6$, and T$_7$. The interactions between the side chain of Arg and the minor groove, along with the C-terminal amide interactions described earlier, while secondary to the main contacts that occur between the
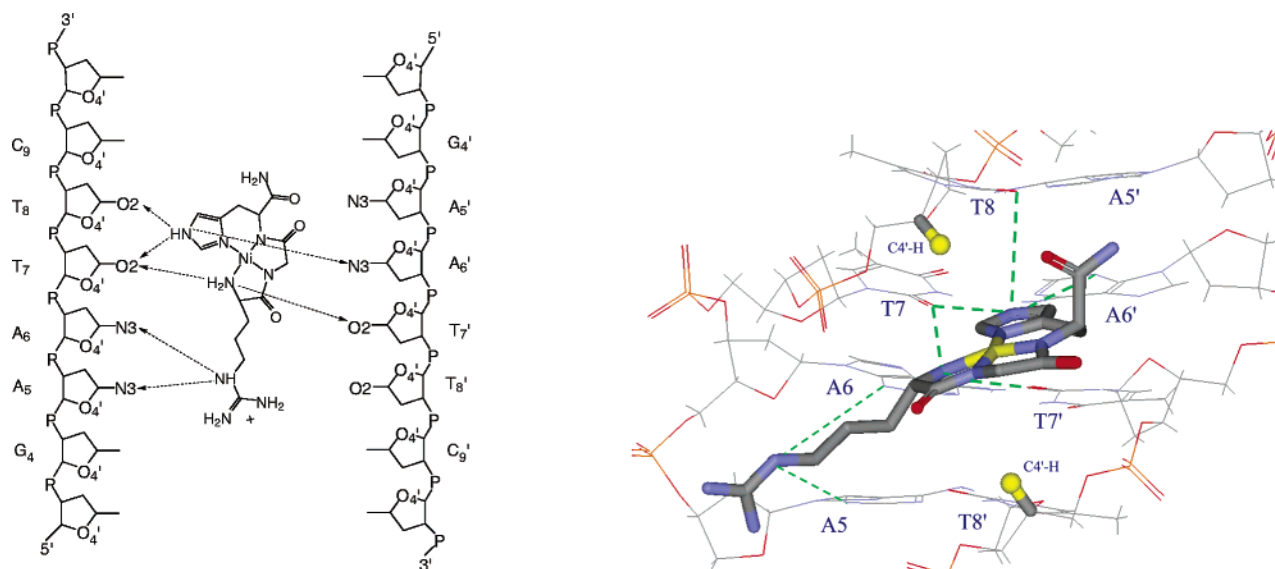
Figure 7. Schematic diagrams of the hydrogen-bond patterns observed upon simulation of Ni(II)·L-Arg-Gly-His bound to d(CGCGAATTCGCG)$_2$. The diagram shown to the right is representative of the average structure observed.

imidazole moiety, the N-terminal amine, and the floor of the minor groove, appear to strengthen the overall binding of the metallopeptide and also assist in maintaining a distinct orientation by providing multiple points of contact.

In the case of Ni(II)·D-Arg-Gly-His, while the overall coordination plane of this metallopeptide isomer was found to be oriented in the DNA minor groove in a fashion comparable to the L-Arg-containing isomer (Figure 6), it bound to the minor groove with less stability and alternated between two distinct sets of contact points (see Supporting Information) while maintaining a near-constant, inflexible structure, as supported by the RMSD calculations. In the two sets of contact points observed, (1) the pyrrole N−H of the His imidazole interacted with the N3 of A6′ while the guanidinium δN−H interacted with the N3 of A_6 or (2) the pyrrole N−H of the His imidazole interacted with the O2 of T_8 while the δN−H of the D-Arg side chain interacted with the O2 of $T_8′$; in these simulations, the His C4 proton of Ni(II)·D-Arg-Gly-His ranged 5−6 Å from the minor-groove $A_6′$-C2 proton. In both (1) and (2) above, the N-terminal peptide protons form an H-bond with only the O2 of $T_7′$, causing the metallopeptide to associate predominantly with one strand of the duplex (see Figure 6). Accompanying these position changes, Ni(II)·D-Arg-Gly-His was observed to slide slightly along the minor groove (±0.5 base pair), unlike the stationary L-Arg isomeric complex. These interactions fundamentally distinguish the D-Arg isomer from the L-Arg isomer and are due to the stereochemistry of the Arg α-carbon, which creates a steric block preventing the formation of interactions with both T_7 O2 residues, as observed with the L-Arg isomer. Accommodating the positional fluctuations discussed and the overall weakened interaction of Ni(II)·D-Arg-Gly-His with the minor groove, the AATT core region was found to be widened slightly to 12−13 Å relative to the unbound AATT core and lacked the snug fit observed with the L-Arg isomer (Figure 6). This weakened interaction and lack of complementary fit is consistent with the decreased affinity of Ni(II)·D-Arg-Gly-His measured through fluorescence displacement. Along with the interactions described above, the C-terminal amide protons of Ni(II)·D-Arg-Gly-His are involved in weak interactions as described also for the L-Arg diastereomeric metallopeptide: transient points of contact are formed with the phosphates of C_9 or the complementary-strand $T_8′$ residue through a small tilting of the complex in the minor groove.

While the guanidinium functional group of the Ni(II)·D-Arg-Gly-His diastereomer participated in the alternating structures described above, along with weak interactions with the phosphates of nucleotides T_7 and $T_8′$, it did so with less flexibility than that of the L-Arg isomer, maintaining a near-constant shape during the course of the simulation due to its weak interaction with the minor groove. As a result, the minor-groove width in proximity to the Arg side chain remained relatively unchanged (Figure 6) in comparison to an unbound oligonucleotide and the starting structure. Despite the weakened interaction between the Arg side chain of Ni(II)·D-Arg-Gly-His and the minor groove, oligonucleotide structural changes that were similar but weaker than those observed and described for Ni(II)·L-Arg-Gly-His occurred within the G/C base pairs flanking the AATT core. This observation suggests that the perturbations in oligonucleotide structure that occur within these flanking regions may be

a consequence of metallopeptide binding to the AATT core as well as proximity of the Arg guanidinium to these regions.

Further experimental support for the differences between the L-Arg and D-Arg metallopeptide isomers noted above is derived from our previous high-resolution DNA restriction fragment cleavage results[39] indicating that, for a given A/T-rich site, the L-Arg isomer modifies only a subset of nucleotides while the D-Arg isomer produces a more uniform distribution of cleavage among all available nucleotides. Thus, the results of both experiment and simulation suggest that the D-Arg isomer, in contrast to the more precisely positioned and tightly held L-Arg isomer, is capable of greater independent motion within the minor groove of a given A/T-rich site, allowing it to slide or position in proximity to multiple C4′-H positions, leading to a decrease in the selectivity of its cleavage patterns.

The simulations described indicate that the selectivity and efficiency of Ni(II)·Arg-Gly-His metallopeptide−minor-groove recognition and binding is dependent upon the formation of direct hydrogen bonds between the floor of the minor groove (the O2 of T residues and the N3 of A residues) and N−H donors contained within the equatorial plane of the metallopeptide, in particular the His imidazole pyrrole N−H and the N-terminal amine protons. In addition, the presence and chirality of the terminal Arg residue assists in this binding process by providing an electrostatic driving force and through the formation of additional, direct stabilizing contacts with the minor-groove floor. With Ni(II)·L-Arg-Gly-His, the full contingent of these interactions leads to an isohelical binding interaction, while with Ni(II)·D-Arg-Gly-His, the stereochemistry of the Arg α-carbon prevents the full formation of these intermolecular interactions, resulting in weakened binding as verified experimentally.

Conclusions and Structural Comparison to Netropsin and Hoechst Dye. The findings presented herein indicate a structural basis for the DNA minor-groove recognition exhibited by Ni(II)·Arg-Gly-His metallopeptides. Selective minor-groove binding by these systems appears to be facilitated by the general structure of A/T-rich regions,[24] including their narrow groove width and perhaps the presence of a spine of hydration and lack of TpA steps, as found in the preferred AATT sequence. With these DNA sites, the His imidazole and N-terminal amine edge of the complex is inserted into the minor groove, forming distinct hydrogen bonds with H-bond acceptor sites on the minor-groove floor. While the above metallopeptide H-bond donors appear to be key determinants of minor-groove binding, their activity is augmented by the side-chain guanidinium of an N-terminal Arg residue, and other peptide moieties as noted. Emphasizing the importance of stereochemical complementarity in the development of DNA minor-groove binding agents, Arg in the context of these metallopeptides leads either to an isohelical, structurally complementary complex (L-Arg) or to attenuated binding affinity through decreased steric compatibility (D-Arg). These findings are supported by both binding and cleavage-based results and assist in explaining the origins of the diastereofacial selectivity of DNA strand scission noted previously[2] with Ni(II)·Gly-Gly-His-modified Hin recombinase (139−190).

Overall, Ni(II)·L-Arg-Gly-His binds to the AATT target

---

(39) Claussen, C. A. Ph.D. Dissertation, Purdue University, West Lafayette, IN, 2003.
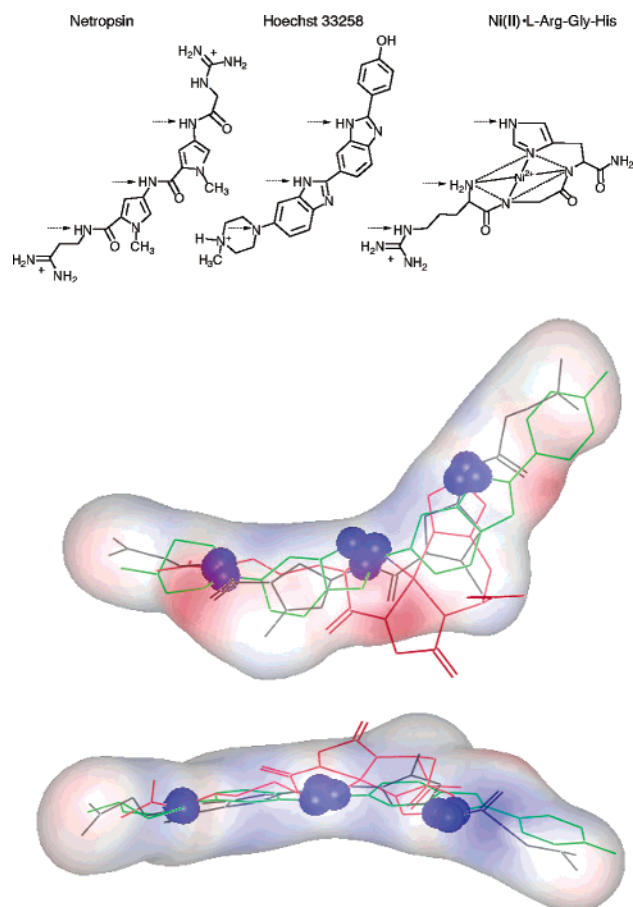
Figure 8. Comparison of the average structure of Ni(II)·L-Arg-Gly-His to netropsin and Hoechst emphasizing the close correspondence of nitrogens (blue spheres) involved in DNA minor-groove recognition [Ni(II)·L-Arg-Gly-His, red; netropsin, black; Hoechst, green].

oligonucleotide, and most likely other sequences, through the formation of complementary hydrogen bonds and steric features reminiscent of the minor-groove binding agent netropsin. Indeed, an analysis of the structure of AATT-bound Ni(II)·L-Arg-Gly-His averaged from the MD simulations presented indicates a surprisingly precise correspondence with those of netropsin (class I binding[34]) and Hoechst 33258 found in structural studies with the same AATT oligonucleotide; in addition to activating the His imidazole as an H-bond donor, the act of Ni(II) complexation and minor-groove binding by Arg-Gly-His produces an alignment of peptide N−H donors that mimics those of netropsin and Hoechst (not all involved in DNA recognition) with an RMS deviation of 0.52 Å. As shown in Figure 8, netropsin, Hoechst, and Ni(II)·L-Arg-Gly-His overlap well with regard to their curvature, thickness, and positioning of N−H donors.

Thus, Ni(II)·Arg-Gly-His metallopeptides, along with A·T-hooks[17] and SPKK motifs,[40] demonstrate how low molecular weight peptides can mimic natural product structural strategies (or vice versa) for DNA minor-groove recognition. While the latter two strategies employ peptide β-turns or Asx bends, respectively, to achieve natural product-like structures, Arg-Xaa-His motifs employ transition metal ions, further underscoring the utility of metal−peptide complexes in the study of biological events.[41] Of particular relevance, given that an Arg-

Thr-His motif is present[5] at the N-terminus of human protamine P2 and that Cu(II) and Ni(II) binding appears to promote the association[5b,c] of a truncated version of this protein to DNA and organization of its secondary structure,[5d] respectively, the question is raised as to the possible role of this metal-bound motif in the DNA minor-groove binding process of protamine and perhaps other proteins containing Xaa-Xaa-His motifs. Curiously, Arg-Thr-His was also selected as one "optimal" tripeptide combination for B-form DNA cleavage in a previous combinatorial study performed in our laboratories.[16] While speculative, these observations suggest that the Cu(II)-bound form of Arg-Thr-His may be a native DNA minor-groove binding motif.

Experimental Section

Materials. All peptides studied were synthesized through standard Fmoc protocols from commercially available side-chain-protected amino acids from Bachem. Peptide purity was monitored on a Varian HPLC employing a Rainin reverse-phase C_{18} column. Water was from a Millipore MilliQ water purification system. DNA oligonucleotides were synthesized and purified by MWG, Inc. (fluoresence titrations) or Trilink Biotech, Inc. (NMR studies).

Fluorescent Intercalator Displacement Studies. Fluorescent intercalator displacement titrations were carried out on a Cary Eclipse spectrofluorometer. Measurements were made with microcuvettes containing an initial solution volume of 200 μL. All fluorescence measurements were taken at a λ_{ex} of 545 nm and a λ_{em} of 595 nm. The instrument was blanked with a solution containing 5 μM ethidium bromide and 10 mM NaCl in 10 mM sodium cacodylate buffer, pH 7.5. Initial 100% F readings were taken after the addition of 2 μL of an annealed oligonucleotide to a final concentration of 1 μM duplex (12 μM base pair). Successive readings of titration points were taken after the addition of 2 μL aliquots of a concentrated, preformed metallopeptide in buffer (10 mM sodium cacodylate, pH 7.5). All fluorescence readings were corrected for volume addition and plotted as a function of fluorescence vs mole fraction of added titrant.

Scatchard analyses of the fluorometry data obtained through the above methods were carried out in standard format by use of the equation [free metallopeptide] = $DNA_T\{[X] - [\Delta F_x/\Delta F_{sat}]\}$ where X is the molar equivalent of metallopeptide vs duplex, ΔF_x is the change in fluorescence at X, ΔF_{sat} is the change in fluorescence at ligand saturation, and DNA_T is the total concentration of duplex. The resulting transformed data was graphed on a plot of ΔF_x/free metallopeptide vs ΔF_x, and the slope of the resulting line gave K_a for those plots resulting in a reasonable fit regression line.

NMR Measurements. All NMR spectra were acquired in buffered 20% D_2O on the Varian Inova 500 MHz NMR spectrometer at the IUPUI NMR Center. On resonance solvent suppression was accomplished by the WET technique with the tuned shaped inversion pulse called the "wet" shape.[42] All 2-D NOE spectra were acquired in hypercomplex mode with 2K (F_2) × 256 (F_1) complex data points and 250 ms mixing time. Data points were extended by forward linear prediction in both dimensions to 4K (F_2) × 1K (F_1) complex data points before Fourier transformation with 80° shifted squared sine bell apodization in both dimensions. Spectra were phased to pure absorption mode. The 1-D spectra were acquired as 4096 complex data points and were Fourier-transformed with zero-filling but without apodization. For both 1-D and 2-D spectra, solvent resonance suppression was enhanced postacquisition by software solvent subtraction.

NMR samples consisted of 2 mM DNA duplex in 700 μL of 20 mM sodium phosphate buffer, pH 7.5, with 10 mM NaCl, and 0.8 mM

(40) Suzuki, M. *EMBO J.* **1989**, *3*, 797−804.

(41) Licini, G.; Scrimin, P. *Angew. Chem., Int. Ed.* **2003**, *42*, 4572−4575.
(42) Smallcombe, S. H.; Patt, S. L.; Keifer, P. A. *J. Magn. Reson. A* **1995**, *117*, 295−303.

sodium [2,2,3,3-^{2}H$_4$]-3-trimethylsilylpropionate as reference to which 5 μL aliquots of a Ni(II)·peptide 1:1 complex in the sample buffer were added to give spectra at DNA duplex:Ni(II)·peptide ratios of 2:1, 1:1, 2:3, and 1:2.

Molecular Modeling and Simulations. All calculations were performed with the following software packages: SPARTAN 5.1,[43] MacroModel 7.0,[44] and AMBER 7.[45] Default settings for these programs were used unless specified otherwise. The coordination complexes described in this paper all contain the basic Gly-Gly-His tripeptide ligand bound to a Ni metal atom; missing force-field parameters were developed for this basic ring system.

Given that only a single X-ray crystallographic study of this system has been published,[38] there exists limited information for purposes of parametrization. One option was to use the core structure as a rigid entity during the simulations, but that is unacceptable because it does not allow for induced-fit changes within the ligand upon DNA binding. In lieu of a full-scale parameter development study, we derived parameters with a single compound by optimizing missing parameters until the root-mean-squared deviation (RMSD) between the calculated and observed geometry was minimized. Missing atomic charges were derived from quantum mechanical calculations (PM3tm) on the X-ray geometry with added hydrogen atoms. A table of the electrostatically fitted charges used and a schematic of the corresponding atom labeling and atom typing is provided as Supporting Information along with the final parameter set. The RMS deviation between the X-ray structure and the AMBER minimized structure for those charges and parameters is 0.257 Å. By use of this set of parameters, an in vacuo simulation was carried out to see if the coordination complex was too rigid or too floppy (a consequence of assigning excessively "soft" torsion parameters). The averaged RMS deviation between the X-ray and computed structures along that trajectory was found to be 0.283 Å. A plot of the RMS deviation versus time is available as Supporting Information. The largest RMS deviation observed was 0.528 Å. There are no guarantees that the existing parameter set is optimal, but it is adequate for our needs; no major structural deformations were found during the simulation and the parameters allow for some induced-fit structural changes during the metallopeptide–DNA binding event.

Assembly of the metallopeptide–DNA complexes was done in the following general manner. Using the atomic coordinates of netropsin-bound d(CGCGAATTCGCG)$_2$ from the Protein Data Bank (reference code 1D86), netropsin was deleted from the minor groove and the metallopeptides were inserted manually with the translation/rotation facility of MacroModel. Bump-checking was turned on to ensure that no overlapping atoms resulted during the docking process and that initial

minor-groove-bound DNA complex was exported to AMBER. To that complex were added the requisite number of Na$^+$ counterions by use of the addIons command in the XLEaP facility of AMBER. The complex was subsequently solvated explicitly by use of the TIP3P water potential inside a central simulation box. The box dimensions ensured solvation extended 10 Å on all sides of the DNA–metallopeptide complex.

The protocol for all MD simulations described herein included the following: (1) The docked metallopeptide–DNA complex with associated Na$^+$ ions and water bath were energy-minimized with 500 steps of conjugate gradient minimizer, with 100 kcal (mol·Å)$^{-1}$ restraints on DNA and counterion positions. During the following three 500-step minimizations, the restraints were relaxed stepwise by 25 kcal (mol·Å)$^{-1}$ per step. Thus the fifth 500-step minimization was performed without restraints. (2) That optimized structure was heated from 100 to 300 K over a time period of 125 ps with a temperature coupling of 0.2 ps while positional restraints of 100 kcal (mol·Å)$^{-1}$ were used for the DNA complex and the counterions. A constant volume was maintained during this process. (3) Three sequential 25 ps MD steps at 300 K were carried out with the gradual loosening of restraints of 25 kcal (mol·Å)$^{-1}$ per step. (4) The system without any restraints was allowed to equilibrate for an additional 2.9 ns; the temperature was allowed to fluctuate around 300 K with a temperature coupling time of 0.2 ps, and the pressure was allowed to fluctuate around 1 bar with a pressure coupling of 0.2 ps. Production runs in excess of 1 ns were carried out following this protocol. For each simulation, 5000 structures were saved to disk for postprocessing by uniformly sampling the trajectory during the production run. All analyses of results were done with the CARNAL and ANAL programs in AMBER.

MM Energy. The gas-phase molecular mechanical (MM) energy was averaged over all the snapshots acquired between 500 and 3000 ps and includes contributions from the electrostatic and van der Waals interactions for the complex, receptor, and ligand. All MM calculations (AMBER) are performed with a nonbonded cutoff of 99 Å and a dielectric constant of 1 in the absence of any solvent or counterions. The receptor and ligand geometries were taken from those of the complex, and thus there is no internal energy (i.e., bonds, angles, and dihedrals) contribution to the net MM average.

Supporting Information Available: Fluorescence displacement titration and Scatchard plots for all oligonucleotide substrates, additional NMR spectra, two tables (force-field parameters and electrostatically fitted charges), a schematic of atom labeling and atom typing, a plot of rmsd vs time used in force field development, metallopeptide + oligonucleotide starting structures, and results of simulations with Ni(II)·D-Arg-Gly-His (PDF). This material is available free of charge via the Internet at http://pubs.acs.org.

JA049875U

(43) Kanemasa, S.; Oderaotashi, Y.; Yamamoto, H.; Tanaka, J.; Wada, E. Spartan; Available from Wavefunction, Inc., 18401 Von Karman, Suite 370, Irvine, CA 92715.
(44) Mohamadi, F.; Richardson, N. G. J.; Guida, W. C.; Liskamp, R.; Lipton, M.; Caufield, C.; Chang, G.; Hendrickson, T.; Still, W. C. *J. Comput. Chem.* **1990**, *11*, 440–467.
(45) Case, D. A.; Pearlman, D. A.; Caldwell, J. W.; Cheatham, T. E., III; Wang, J.; Ross, W. S.; Simmerling, C. L.; Darden, T. A.; Merz, K. M.; Stanton, R. V.; Cheng, A. L.; Vincent, J. J.; Crowley, M.; Tsui, V.; Gohlke, H.; Radmer, R. J.; Duan, Y.; Pitera, J.; Massova, I.; Seibel, G. L.; Singh, U. C.; Weiner, P. K.; Kollman, P. A. AMBER 7; University of California, San Francisco, CA, 2002.